processes

MDPI

Article

Prussian Blue–Alumina as Stable Fenton-Type Catalysts in Textile Dyeing Wastewater Treatment

Lucila I. Doumic [1,2,*], Ana M. Ferro Orozco [1], Miryan C. Cassanello [3] and María A. Ayude [1,2,*]

[1] Instituto de Investigaciones en Ciencia y Tecnología de Materiales (INTEMA), CONICET-UNMdP, Mar del Plata B7606, Argentina; micaela.ferro@fi.mdp.edu.ar
[2] Departamento de Ingeniería Química y en Alimentos (DIQyA), UNMdP, Mar del Plata B7600, Argentina
[3] Instituto de Tecnología de Alimentos y Procesos Químicos (ITAPROQ), CONICET-UBA, Ciudad Autónoma de Buenos Aires C1428, Argentina
* Correspondence: luciladoumic@fi.mdp.edu.ar (L.I.D.); mayude@fi.mdp.edu.ar (M.A.A.)

Abstract

Textile dyeing effluents are characterized by recalcitrant organics and high salinity, requiring robust pretreatments prior to biological polishing. The heterogeneous Fenton-type (HFT) oxidation over Prussian Blue nanoparticles supported on γ-alumina (PBNP/γ-Al_2O_3) was investigated in a liquid batch-recycle packed-bed reactor treating a synthetic textile wastewater (STW) reproducing an industrial dye bath with the Reactive Black 5 (RB5) dye, together with simplified RB5 and RB5 + NaCl matrices. Hydrogen peroxide decay followed pseudo-first-order kinetics. Using fixed initial doses (11, 20, 35 mmol L^{-1}), the catalyst exhibited an early adaptation phase and then reproducible operation: from the fourth reuse onward, both the H_2O_2 decomposition rate constant and DOC removal varied by <10% under identical conditions. Among matrices, STW exhibited the highest oxidant efficiency. With an initial H_2O_2 dose of 11 mmol L^{-1}, the treatment enabled complete discoloration and produced effluents with negligible toxicity. Increasing the initial dose to 20 or 35 mmol L^{-1} did not improve treatment and led to a decrease in the hydrogen peroxide decomposition rate with reuses and loss of PB ν(C≡N) Raman bands, indicating surface transformation. Overall, PBNP/γ-Al_2O_3 demonstrated reproducible activity and structural resilience in saline, dyeing-relevant matrices at H_2O_2 doses that preserve catalytic integrity, confirming its feasibility as a stable and reusable pretreatment catalyst for saline dyeing effluents, and supporting its integration into hybrid AOP–biological treatment schemes for dyeing wastewater.

Keywords: advanced oxidation processes (AOPs); heterogeneous Fenton-type oxidation Reactive Black 5; saline matrix; saline textile dyeing wastewater; batch-recycle packed-bed reactor; catalyst reuse stability

check for updates

Academic Editor: Maria Victoria López Ramón

Received: 7 October 2025
Revised: 30 October 2025
Accepted: 5 November 2025
Published: 11 November 2025

Citation: Doumic, L.I.; Ferro Orozco, A.M.; Cassanello, M.C.; Ayude, M.A. Prussian Blue–Alumina as Stable Fenton-Type Catalysts in Textile Dyeing Wastewater Treatment. *Processes* **2025**, *13*, 3656. https://doi.org/10.3390/pr13113656

Copyright: © 2025 by the authors. Licensee MDPI, Basel, Switzerland. This article is an open access article distributed under the terms and conditions of the Creative Commons Attribution (CC BY) license (https://creativecommons.org/licenses/by/4.0/).

1. Introduction

Textile dyeing and finishing operations generate saline effluents with intense color, high salinity, and biologically recalcitrant organics, including surfactants and auxiliaries, which challenge conventional treatments [1]. Azo dyes such as Reactive Black 5 (RB5) are particularly problematic due to their high stability and low biodegradability, making the development of robust pretreatment strategies a research priority [2]. In typical cotton dyeing, industry surveys report ~80% dye retention to fabric for RB5, implying ~20% remains in the spent bath and ultimately enters wastewater alongside substantial salt loads and additives [3].

Advanced oxidation processes (AOPs) are widely studied because they generate highly reactive hydroxyl radicals capable of non-selectively degrading a broad spectrum of organic pollutants [4]. Within AOPs, Fenton chemistry is attractive due to its high oxidizing power, operational simplicity, and ability to increase effluent biodegradability [5]. Nevertheless, in textile dyeing effluents, homogeneous Fenton exhibits major limitations: precipitation of ferric organic complexes with dyes and auxiliaries, and scavenging of hydroxyl radicals by salts, especially chloride and bicarbonate/carbonate ions, which transform •OH into less potent, more selective radical species and restrict mineralization even when color removal is high [6–8]. Furthermore, its industrial scalability is constrained by the need for strict pH and reagent control, high chemical costs, and the generation of large volumes of ferric sludge [9,10]. Similar concerns regarding operating costs and sludge disposal have been consistently highlighted in critical reviews [11]. Thus, the Fenton approach is typically more effective as pretreatment to raise biodegradability and reduce toxicity before biological polishing, rather than as a standalone deep mineralization step in highly saline, organic-rich matrices. Heterogeneous Fenton-type (HFT) systems immobilize iron on solid supports, offering practical advantages such as easier catalyst recovery, lower sludge generation, the possibility of catalyst reuse, and operation without external irradiation, provided the catalyst retains activity and structural integrity under the complex matrices characteristic of dyeing baths [10–12]. In recent years, the use of fixed and fluidized-bed reactors has further highlighted the potential of HFT processes for continuous treatment, although catalyst deactivation and long-term stability remain central challenges [11,13].

Iron-oxide heterogeneous Fenton catalysts such as Fe_3O_4, goethite, and FeOOH often show a gradual loss of activity when reused with real textile effluents: iron can leach over cycles, and the surface can change, which makes it harder to keep the reaction truly heterogeneous and complicates catalyst reuse [9]. In addition to radical scavenging, high-salinity matrices may promote active-site blocking and inorganic scaling, leading to surface coverage that hinders interfacial catalysis [14]. Supporting iron oxides on solid matrices helps with recovery, improves mechanical robustness, and can limit iron release, although some performance loss may still occur in the presence of electrolytes [9]. Among emerging catalysts, Prussian Blue (PB) and its analogues are attractive due to their open-framework structure and mixed valence Fe(II)/Fe(III) centers, whose defect chemistry allows structural robustness under redox cycling. In energy-storage systems, PB frameworks exhibit near-zero-strain behavior and high cycling stability in aqueous systems; >98% capacity retention over $\geq$200 electrochemical cycles has been reported when used as electrode materials [15], illustrating an intrinsically robust architecture that motivates their evaluation for HFT catalysis. Their long-term stability depends on intrinsic structural features such as $[Fe(CN)_6]$ vacancies, coordinated water and ion interactions, which are well established in the energy storage field but remain scarcely explored in heterogeneous Fenton-type processes for wastewater treatment [16,17]. When immobilized on γ-Al_2O_3, PB nanoparticles (PBNP) combine the framework stability of PB with the mechanical and hydrodynamic robustness of the support, forming an eggshell-type catalytic layer previously proven active and reusable in HFT oxidation of model compounds in both batch and continuous configurations [6,18,19]. Nevertheless, their application to realistic textile effluents is still unexplored. For dyeing effluents, catalysts must withstand high salinity and auxiliaries without loss of activity or reusability [20]. Thus, assessing catalyst stability and process efficiency in synthetic effluents representative of local industry becomes critical to validate the feasibility of Prussian Blue-based HFT systems.

This study addresses these knowledge gaps by evaluating PBNP/γ-Al_2O_3 as HFT catalysts for a synthetic cotton-textile wastewater (STW) formulated to reproduce an industrial dye bath from local practice. We adopt a stepwise complexity strategy that considers

RB5 alone, RB5 with sodium chloride at the same chloride level as the synthetic wastewater, and the complete matrix with auxiliaries. The influence on discoloration, dissolved organic carbon removal, oxidant efficiency defined as carbon removed per mole of hydrogen peroxide consumed, catalyst stability and reuse, iron release, and toxicity was assessed.

2. Materials and Methods

2.1. Synthetic Cotton-Textile Dyeing Wastewater (STW) Preparation and Characterization

The STW used in this study was prepared in the laboratory following a methodology adapted from Hanela et al. [3] to simulate the effluent produced during the dyeing and rinsing of 100% cotton fabric. The preparation procedure reproduced the composition of typical dye baths by combining Reactive Black 5 (RB5) with auxiliary chemicals commonly used in industrial cotton dyeing, including humectants, detergents, sodium chloride, sodium carbonate, and a commercial softener. The RB5 dye (C.I. No. 20505; Sigma-Aldrich, St. Louis, MO, USA), surfactant, and detergent were provided by a local textile industry located in Mar del Plata, Argentina. A commercial softener (Vivere Classic) was used, along with common coarse salt (NaCl). Analytical grade reagents, including Na_2CO_3, NaOH, and glacial acetic acid, were also employed.

The STW was centrifuged before characterization, which included the determination of UV–Vis spectrum, pH, conductivity, toxicity, and the concentrations of RB5, chloride, and dissolved organic carbon (DOC). Based on the results of this characterization, model aqueous solutions containing RB5 and RB5 with NaCl were prepared to serve as references for comparative analysis. The concentrations of RB5 and NaCl in these solutions matched those measured in the STW.

2.2. Catalysts Synthesis and Characterization

PBNP/γ-Al_2O_3 was prepared following our previous procedure [18]. Briefly, an aqueous PB dispersion was obtained by contacting $FeCl_3$ with $K_3[Fe(CN)_6]$ in the presence of H_2O_2 as a reducing agent. The resulting PBNP was immediately immobilized onto γ-Al_2O_3 spheres by impregnation. The composite was dried at low temperature to preserve the PB framework (no calcination). The total Fe content was ~0.4 wt%, and the active PB layer exhibited an eggshell distribution over the alumina spheres, with irregular PBNP domains well below ~100 nm, as reported previously for this formulation. Fresh catalyst beds were conditioned in situ by circulating an acidic solution (pH 2) at 75 °C prior to the first run to ensure the removal of unreacted species and enhance stability.

Fresh and reused catalyst samples were analyzed by X-ray diffraction (XRD), grazing-incidence XRD (GIXRD), and Raman spectroscopy. Powder XRD (Cu Kα, λ = 1.5406 Å) was recorded over $2\theta \approx 5$–80° with fine steps ($\leq 0.02^\circ$) and sufficient counting to probe weak reflections. To enhance surface sensitivity toward the thin PB layer, GIXRD was collected at fixed, shallow incidence (typically 0.5–1.0°).

Raman spectra were acquired using a Renishaw InVia Reflex spectrometer (Renishaw plc, Wotton-under-Edge, Gloucestershire, UK) equipped with a charge-coupled device (CCD) detector (1040 × 256 pixels). Excitation was provided by a 785 nm diode laser (nominal output 300 mW) combined with a 1200 grooves mm^{-1} diffraction grating. To prevent thermal or photochemical damage to the sample, the incident laser power was maintained below 10% of the maximum output. A 50× Leica metallurgical objective (Leica Microsystems, Wetzlar, Germany; numerical aperture = 0.5, working distance = 8 mm) was employed for both excitation and signal collection. Spectra were typically acquired in 30s with a minimum of three accumulations to improve the signal-to-noise ratio.

2.3. Heterogeneous Fenton-Type (HFT) Treatment

To evaluate the performance of the HFT catalyst (PBNP/γ-Al_2O_3) across systems of increasing complexity, we adopted a stepwise approach: (i) aqueous RB5, (ii) RB5 with NaCl at the same chloride level as the synthetic wastewater, and (iii) the synthetic cotton-textile dyeing wastewater (STW), under identical operating conditions unless otherwise noted. HFT experiments were then carried out in a liquid batch-recycle reactor, schematically shown in Figure 1. The reactor consisted of a glass tube (internal diameter: 11 mm) with a catalytic section containing 2 g of randomly packed PBNP/γ-Al_2O_3. The pre- and post-packing sections contained inert glass spheres of 3 mm diameter, which served to hold the catalyst. The whole system (reservoir, reactor, and tubing) was submerged inside a thermostatic bath to maintain the temperature at 75 °C. The reaction temperature was selected based on previous studies [19,21], which demonstrated that this catalyst exhibits enhanced activity at elevated temperatures. Under these conditions, the reaction proceeds predominantly through oxidative pathways rather than being limited by adsorption phenomena. A condenser was placed on the reservoir to minimize evaporation losses. A volume of 175 mL of centrifuged STW, RB5, or RB5 with NaCl aqueous solutions was introduced into the reservoir to start each test. The initial pH was adjusted to 3. H_2O_2 was added and allowed to mix. The initial sample was collected, and the liquid flow (1.15 L h^{-1}) through the reactor was initiated using a peristaltic pump. Each reaction cycle lasted 270 min, and all experiments were conducted for this duration consistently across matrices to ensure a uniform endpoint for performance evaluation. Liquid samples were periodically withdrawn from the reservoir and immediately analyzed for pH, UV–Vis spectrum, RB5, H_2O_2, and DOC concentrations. Oxidant efficiency, defined as the time-averaged ratio between DOC removal and H_2O_2 decomposition over each complete cycle, was estimated for certain relevant conditions. DOC removal was obtained from the initial and final DOC measurements, while the cumulative decomposed H_2O_2 was estimated from the pseudo-first order model fitted to the H_2O_2 data. This definition captures the overall use of the oxidant toward organic carbon removal across the entire reaction interval, without relying on pointwise rate ratios or discretized calculations.

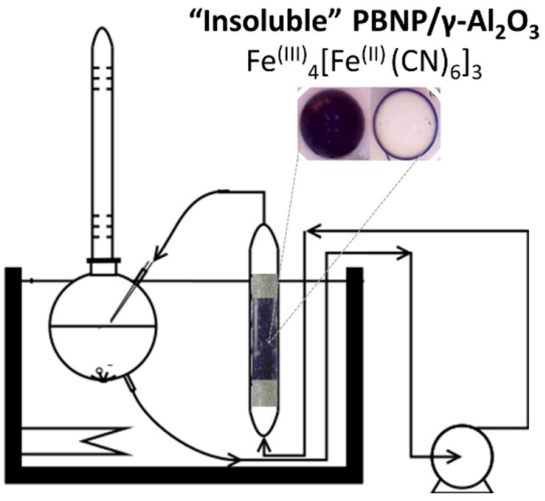


Figure 1. Scheme of the facility used for the heterogeneous Fenton-type (HFT) process carried out in a liquid batch-recycle reactor.

A fresh PBNP/γ-Al_2O_3 bed was used for the first cycle of each matrix (RB5, RB5 + NaCl, STW). Catalyst stability was assessed by operating consecutive cycles on the same bed under identical conditions within each matrix.

2.4. Stable Operation Criteria

We defined stable operation as occurring when both the apparent H_2O_2 decomposition rate constant (k_{H2O2}) and DOC removal varied by <10% between consecutive 270 min HFT cycles. HFT treatment of each matrix (RB5, RB5 + NaCl, STW) began with a fresh catalyst. Unless otherwise noted, results refer to operation after the initial adaptation cycle, when the system reached reproducible performance, and are reported as the mean of the cycles conducted under stable operation.

2.5. Analytical Techniques

H_2O_2 concentration was determined colorimetrically using the Glycemia enzymatic test (Wiener Lab.). The method's principle is based on the reaction between H_2O_2, 4-aminophenazone (4-AP), and phenol in the presence of peroxidase (POD) to form a red quinoneimine. The working reagent (pH = 7.4 ± 1) was prepared according to the manufacturer's protocol and contained POD (≥400 U L^{-1}), 4-AP (1.25 mmol L^{-1}) in Tris buffer, and phenol (2.75 mmol L^{-1}). For each measurement, 20 µL of the sample was mixed with 2 mL of the working reagent, and the absorbance of the resulting colored solution was recorded at 505 nm using a Shimadzu UV-1800 spectrophotometer (Shimadzu Corporation, Kyoto, Japan). Hydrogen peroxide concentration was then quantified from the corresponding calibration curve. Color after 1:40 dilution was visually assessed. A Shimadzu UV-1800 spectrophotometer was used to obtain the UV–Vis spectra between 190 and 800 nm. Total dissolved ("free") iron was assessed by measuring the total iron content of filtered samples with the o-phenantroline method [22]. PB species were monitored by UV–Vis spectroscopy: a broad absorption near 700 nm is indicative of colloidal PBNP. The presence of ferrocyanide and/or ferricyanide ions was tracked spectrophotometrically following the procedure described by Chakrabarti and Roberts [23]. The absorbance at 590 nm was correlated with RB5 concentration. DOC was measured in a Shimadzu TOC-VCPN analyzer (Shimadzu Corporation, Kyoto, Japan). Toxicity was determined by considering the inhibition of microbial respiration in a closed respirometer, following ISO 8192 [24], using sodium acetate as a biodegradable substrate. Oxygen uptake rate (OUR) inhibition was calculated relative to a control without toxic compounds.

3. Results

3.1. STW Characterization

The STW reproduced the composition of a cotton dyeing bath showing a moderate organic load (DOC = 149 mg L^{-1}) and an RB5 concentration of 135 mg L^{-1}. The solution was highly saline (conductivity of 16 mS cm^{-1}) and slightly basic (pH 8.5). An intense blue–black color with a maximum absorbance at 590 nm was observed and remained detectable after a 1:40 dilution. Toxicity was negligible as indicated by the low inhibition of microbial respiratory activity (4.5 ± 1.8%). These results are summarized in Table 1.

Table 1. Characterization of the synthetic textile wastewater.

Parameter	Unit	Value
Dissolved Organic Carbon (DOC)	mg_C L^{-1}	149
RB5 concentration	mg L^{-1}	135
Cl^- concentration	g L^{-1}	10
Color after a dilution of 1:40		visible
pH		8.5
Conductivity	mS cm^{-1}	16
TOXICITY—Inhibition of the Respiratory Activity (I_{SOUR})	%	4.5 ± 1.8

3.2. HFT Oxidation

As an initial step, the oxidation of an aqueous RB5 solution (135 mg L^{-1}, matching the concentration in the STW, $[DOC]_0$ = 42 mg L^{-1}) was investigated using a fresh 2 g catalytic bed, which was reused in consecutive 270 min cycles under identical conditions (T = 75 °C, pH = 3, liquid flow rate = 1.15 L h^{-1}). Unless otherwise specified, the initial H_2O_2 concentration was fixed at 11 mmol L^{-1}, corresponding to the approximate theoretical stoichiometric requirement for the initial RB5 concentration. Representative temporal profiles of normalized RB5 concentration and H_2O_2 consumption under stable operation are shown in Figure 2. Complete discoloration was consistently achieved within approximately 90 min. Runs were extended to 270 min to allow near-complete H_2O_2 consumption and additional DOC removal; >95% of the oxidant was consumed, and DOC removal reached 14.2 ± 0.6 mg L^{-1} by the end of each run (Table 2).

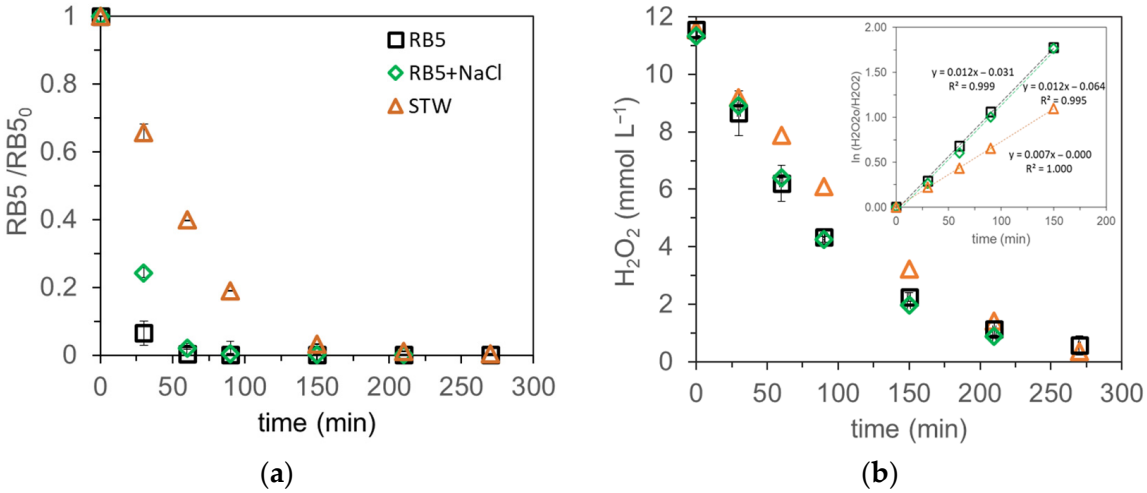


Figure 2. Temporal profiles under stable operation (cycles ≥ 4) of (**a**) normalized RB5 and (**b**) H_2O_2 concentrations after achieving stable performance. Inset: Linear regressions based on pseudo-first order kinetics for H_2O_2 decomposition.

Table 2. Amount of DOC removed and oxidant efficiency (mmol DOC removed per mmol H_2O_2 consumed) under stable operation for RB5, RB5 + NaCl, and STW.

System	Amount of DOC Removed (mg L^{-1})	Oxidant Efficiency ($mmol_{DOC}$ $mmol_{H2O2}{}^{-1}$)
RB5	14.2 ± 0.6	0.01136
RB5 + NaCl	11.0 ± 0.6	0.00867
STW	14.8 ± 0.9	0.01607

To evaluate chloride effects typical of dyeing baths, the experiments were repeated with RB5 + NaCl at the chloride concentration measured in STW (10 g L^{-1} Cl^-). The presence of NaCl did not significantly affect the oxidant decomposition rate (Figure 2b). In contrast, both DOC removal and discoloration rate were lower when chloride was present (Table 2 and Figure 2a). The amount of DOC removed decreased from 14.2 ± 0.6 mg L^{-1} without salt to 11.0 ± 0.6 mg L^{-1} with 10 g L^{-1} NaCl, resulting in a decrease in the oxidant efficiency (DOC removed per mole of H_2O_2 consumed) for RB5 + NaCl relative to RB5 (Table 2). These trends suggest that, although the surface-catalyzed H_2O_2 decay proceeds at similar apparent rates, fewer oxidants are effectively utilized for carbon removal in the saline matrix.

The representative temporal profiles for STW are also included in Figure 2. Complete discoloration was achieved within 210 min, and the oxidant was nearly depleted by the

end of the treatment, albeit at a slower rate. Despite the slower oxidant decay, the amount of DOC removed was comparable, or even higher, than that of RB5, so STW displayed the highest oxidant efficiency among the three matrices (Table 2). In addition, toxicity tests on the treated STW obtained with the initial oxidant dose of 11 mmol L^{-1} showed only minor inhibition of microbial respiration (2.0 ± 0.9%), indicating the absence of toxicity under these conditions.

3.3. Reuse, Catalyst Stability, and Initial Oxidant Dose

This section examines the catalytic performance of PBNP/γ-Al_2O_3 upon its reuse in RB5, RB5 + NaCl, and STW oxidation using an initial H_2O_2 dose of 11 mmol L^{-1}, as well as the influence of the initial oxidant dose. For all matrices, H_2O_2 decay followed a pseudo–first-order kinetic model ($R^2 > 0.981$), as shown in the inset of Figure 2b for the stable operation. The apparent rate constants, k_{H2O2}, calculated for all reuse cycles conducted with $[H_2O_2]_0$ = 11 mmol L^{-1} are reported in Figure 3. After an initial decline, k_{H2O2} stabilized from the fourth reuse onward. In RB5 oxidation, it yielded a value of (1.12 ± 0.06) × 10^{-2} min^{-1} ($R^2 > 0.9905$). In RB5 + NaCl experiments, it remained essentially unchanged at (1.14 ± 0.05) × 10^{-2} min^{-1} ($R^2 > 0.9911$). In STW treatment, k_{H2O2} stabilized at a value of (6.6 ± 0.6) × 10^{-3} min^{-1} ($R^2 > 0.9843$), lower than in RB5 and RB5 + NaCl systems. The initial gradual decay in k_{H2O2} may be influenced by a transient, homogeneous Fenton-type contribution from leached species operating during the first reused cycles. This contribution dissipated once stable operation was attained: at the end of each cycle, UV-vis spectra indicated negligible release of PB or ferri/ferrocyanide species and total dissolved iron was always below 0.25 mg L^{-1}, in line with previous reports on PB/Al_2O_3 stability [18,21]. Figure 4 shows the amount of DOC removed at the end of each cycle conducted with $[H_2O_2]_0$ = 11 mmol L^{-1}. Variations in the first reuse cycles reflected the transition toward catalyst stabilization, and stable operation was consistently attained from the fourth cycle onward.

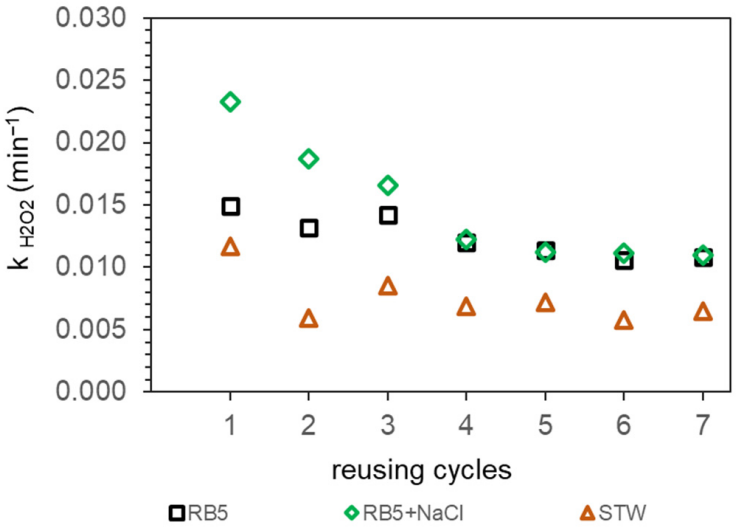


Figure 3. Pseudo-first order reaction rate constants for the decomposition of H_2O_2 across consecutive reuse cycles (270 min each) during HFT of STW, RB5, and RB5 + NaCl using $[H_2O_2]_0$ = 11 mmol L^{-1}.

Macroscopically, the catalyst color changed from deep blue (fresh) to lighter blue (used) after operation, suggesting superficial modifications but not evidencing bulk PB loss. Consistently, no measurable release of PB particulates into the liquid phase was detected across matrices and reuse cycles within our detection limits.

XRD/GIXRD and Raman were performed on fresh and reused samples. Neither powder XRD nor GIXRD resolved PB reflections on PBNP/γ-Al_2O_3; only γ-Al_2O_3 peaks

were observed. This is consistent with a low-loading, nanometric, surface-dispersed PB phase on γ-Al_2O_3 (total Fe ≈ 0.4 wt%, egg-shell distribution of the active layer, and PBNP of irregular shape with sizes well below ~100 nm) [18], for which weak/broadened PB reflections are expected to fall below XRD detection limits and be masked by the strong alumina background. Raman spectroscopy (Figure 5) complements XRD/GIXRD for the low-loading, nanometric PBNP phase. Fresh PBNP/γ-Al_2O_3 displayed the characteristic ν(C≡N) bands of PB in the expected region (~2154 cm^{-1} and ~2091 cm^{-1}), while features around ~2124–2131 cm^{-1} and ~2063–2091 cm^{-1} are diagnostic for $[Fe^{III}(CN)_6]^{3-}$ and $[Fe^{II}(CN)_6]^{4-}$ environments, respectively [25,26]. After reuse in RB5 + NaCl and STW, the ν(C≡N) bands remain but show lower intensity and slight broadening, a change compatible with thin surface deposits, minor surface adjustments, and/or partial early loss of ferro/ferricyanide that attenuates the PB Raman response without elimination of the PB framework.

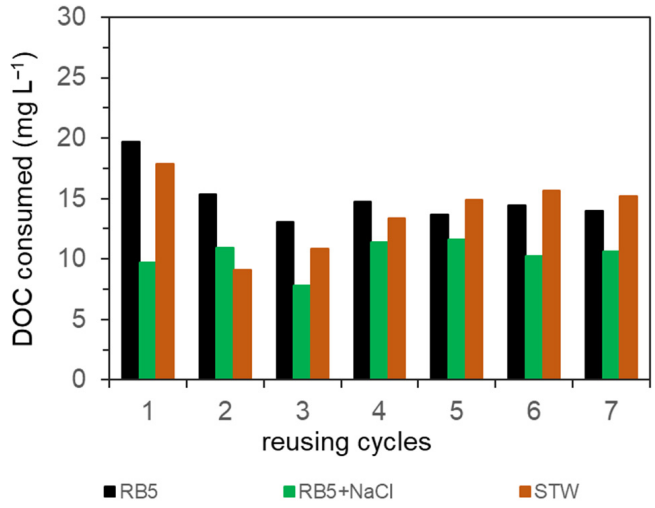


Figure 4. Extent of DOC removal at the end of each 270 min reuse cycle during the HFT treatment of STW, RB5, or RB5 with NaCl aqueous solutions using $[H_2O_2]_0$ = 11 mmol L^{-1}.

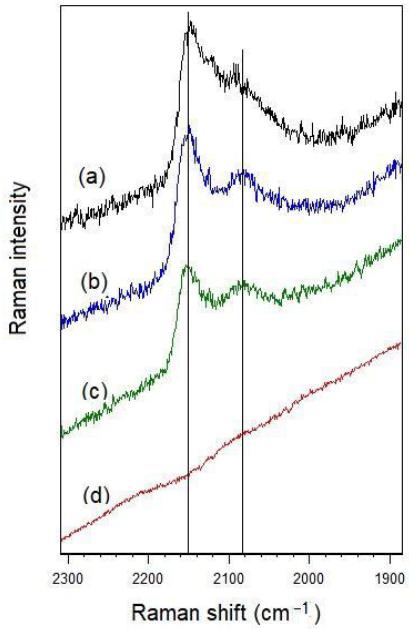


Figure 5. Raman spectra (785 nm excitation) of PBNP/γ-Al_2O_3: (a) fresh; (b) reused in RB5 + NaCl; (c) reused in STW (both under stable operation at $[H_2O_2]_0$ = 11 mmol L^{-1}); (d) after operation at higher initial oxidant doses (20–35 mmol L^{-1}).

To assess the influence of the initial H_2O_2 concentration, a fresh catalytic bed was first stabilized through three reuse cycles at $[H_2O_2]_0$ = 11 mmol L^{-1}. The oxidant dose was then increased to 20 mmol L^{-1} in the fourth reuse, to 35 mmol L^{-1} in the fifth and sixth reuses, and finally reduced again to 20 mmol L^{-1} in the seventh reuse. Discoloration and DOC removal exhibited no significant improvement at higher initial doses, and persistent bubbles were observed over the packed bed. Figure 6 shows that the k_{H2O2} steadily decreased with reuses, suggesting that catalytic activity was not fully sustained upon reuse. Raman analyses of catalysts reused at the higher doses exhibited negligible intrinsic features in the 100–1200 cm^{-1} region, and Figure 5 shows no clearly resolved ν(C≡N) bands in the 2150–2050 cm^{-1} window. This loss of the PB-related bands is consistent with a surface transformation of the PB layer and helps explain the drop in k_{H2O2}.

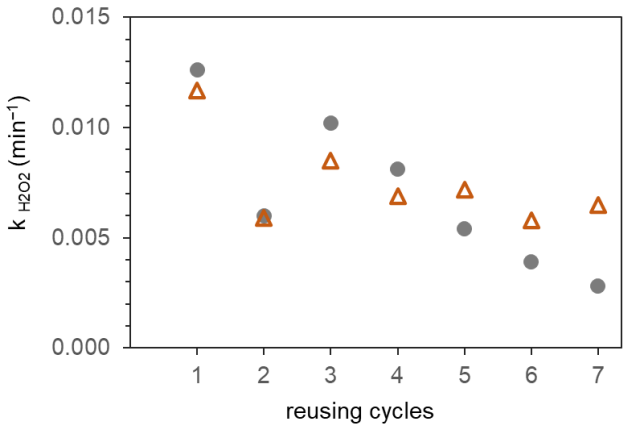


Figure 6. Pseudo-first order reaction rate constants for the decomposition of H_2O_2 across consecutive reuse cycles during HFT of STW under identical conditions, while varying the initial oxidant dose: (△) $[H_2O_2]_0$ = 11 mmol L^{-1} in all reuses, (●) $[H_2O_2]_0$= 11 (1st to 3rd); 20 mmol L^{-1} (4th reuse), 35 mmol L^{-1} (5th–6th), and back to 20 mmol L^{-1} (7th).

4. Discussion

In all systems, treatments conducted with an initial H_2O_2 concentration of 11 mmol L^{-1} exhibited a moderate decline in performance during the first reuse cycles, after which performance stabilized. From the fourth reuse onward, both k_{H2O2} and DOC removal varied by <10%, meeting the stability criterion (Figures 3 and 4). This trend agrees with prior results for PBNP/γ-Al_2O_3 in HFT of a model azo dye, which showed early-cycle stabilization [18]. This behavior indicates an intrinsic catalyst response rather than a matrix-specific effect. This is likely related to the defect chemistry of Prussian Blue (PB); vacancies in $Fe(CN)_6$ generate Fe centers that lack their full set of CN ligands and tend to bind water, yielding surface domains that are mechanically and chemically weaker and undergo mild, self-limited reorganization (local hydrolysis, coordination rearrangement, and desorption of labile species) under operating conditions until a more robust state is reached [27]. In line with defect-engineering studies, controlling (typically lowering) vacancy density and coordinated water improves framework robustness and mitigates metal dissolution in aqueous environments [15]. Consistently, in our experiments, a limited detachment of ferro/ferricyanide was detected in the first reuse cycles, which is consistent with vacancy-driven hydration at subcoordinated metal sites. This early CN-loss increases the local vacancy density and promotes a mild surface reorganization under operating conditions. Subsequently, the system reaches a steady state: dissolved Fe remains low and the catalytic performance becomes reproducible from cycle to cycle. This sequence agrees with the defect chemistry of PB and PB analogues, and with reports of surface self-reconstruction under operation [27].

In RB5 + NaCl, the apparent H_2O_2 decomposition rate remained essentially unchanged relative to RB5, whereas DOC removal and oxidant efficiency decreased (Figures 3 and 4; Table 2). This outcome is consistent with the role of chloride in saline matrices: Cl^- scavenges HO• to form chlorine-derived radicals (e.g., Cl•/Cl_2•$^-$), which are generally less effective than HO• for DOC removal [7]. The magnitude of the decrease in the amount of DOC removed and oxidant efficiency upon adding NaCl is limited within our system (i.e., we observe a reduction relative to RB5, but not a collapse), which suggests that saline effects are partly moderated at the interface. A plausible explanation is that the negatively charged PB framework electrostatically disfavors local Cl^- accumulation near reactive domains, thereby limiting direct chloride participation in radical scavenging at the solid–liquid interface. This concept was recently discussed by Li et al. [14] as a general interfacial strategy for high-salinity AOPs.

On the other hand, once stable operation was achieved in the STW treatment, the apparent k_{H2O2} was lower than in RB5 and RB5 + NaCl systems, while the amount of DOC removed was comparable to, or even higher, yielding the highest oxidant efficiency among the three matrices (Figures 3 and 4; Table 2). This inverse relationship between apparent H_2O_2 decomposition rate and oxidant efficiency suggests that, in complex effluents, surface and radical reactions are partially decoupled. Two complementary effects can explain the results obtained. First, auxiliary chemicals present in the STW (e.g., surfactants, softeners) can adsorb onto the catalyst surface and partially block sites that catalyze non-productive H_2O_2 decomposition, thereby reducing parasitic oxidant loss and promoting oxidant use towards organic oxidation at the liquid–solid interface [28]. Second, oxidant efficiency is controlled by kinetic competition between organics, oxidants, and inorganic scavengers in hydroxyl-radical-dominated systems. As highlighted by Li et al. [14], the extremely high rate constants of •OH reactions make the outcome highly sensitive to matrix composition. The higher initial background DOC in the STW matrix increases the probability that •OH reacts with bulk organics, improving the fraction of oxidant that effectively contributes to carbon removal [29]. Taken together, the competitive and spatially confined reactions explain why apparent oxidant decomposition rates may decrease while carbon removal efficiency improves in complex matrices. This stable and moderately inhibited behavior is consistent with a catalyst that retains its structure while undergoing only minor surface restructuring. The non-detection of PB by XRD/GIXRD (expected for a thin, low-loading PB layer on γ-Al_2O_3) together with the persistence of Raman ν(C≡N) bands, supports a preserved PB framework undergoing mild surface reorganization, consistent with the stable kinetics observed across cycles.

In contrast, exposure of the catalytic bed to higher H_2O_2 concentrations (20–35 mmol L^{-1}) during the STW treatment caused its progressive deactivation. The macroscopic bleaching/browning of the bed, together with the decline in k_{H2O2} (Figure 6), indicates a surface transformation of the PB layer under these higher oxidant doses. No PB-related bands were resolved in the 2150–2050 cm^{-1} region, and the absence of the ν(C≡N) vibration suggests that Raman-active PB was no longer detected at the surface, either due to its conversion into Fe(III) domains or to coverage by secondary phases that depress the PB signal below detection. In the 100–1200 cm^{-1} region, no distinct Fe–O bands were discernible, as expected for poorly crystalline Fe(III) (oxy)hydroxides at low loading, whose Fe–O bands are intrinsically weak and broadened and, under the present acquisition settings, remain indistinguishable from the support baseline of γ-alumina (which is essentially Raman-inactive in that region) [30,31]. Despite the decrease in k_{H2O2} with reuses, a greater amount of H_2O_2 was decomposed compared to the treatments conducted at 11 mmol L^{-1}. This was accompanied by continuous generation and persistence of oxygen bubbles over the packed bed, which may have imposed local mass-transfer limitations and transient

site blocking [19]. Thus, increasing the initial oxidant concentration mainly enhanced non-productive H_2O_2 decomposition rather than mineralization, yielding a decrease in oxidant efficiency.

5. Conclusions

The heterogeneous Fenton-type (HFT) oxidation over Prussian Blue nanoparticles supported on γ-alumina (PBNP/γ-Al_2O_3) demonstrated stable and reproducible performance in saline textile dyeing matrices representative of cotton dyeing baths. At an initial H_2O_2 dose of 11 mmol L^{-1}, the catalyst maintained reproducible performance through multiple reuse cycles, with variations below 10% in both the apparent H_2O_2 decomposition rate constant and DOC removal after an initial adaptation phase, confirming the structural robustness of the PB framework under repeated uses. The process achieved complete discoloration with negligible effluent toxicity. Higher H_2O_2 doses (20–35 mmol L^{-1}) led to surface transformation, as evidenced by the disappearance of the PB ν(C≡N) Raman bands and the macroscopic bleaching/browning of the bed. Accordingly, the apparent H_2O_2 decomposition rate constant decreased with reuse.

These findings highlight the importance of controlling oxidant dosage to preserve the integrity of the low-loading PB layer and maintain high oxidant efficiency. They also point to practical routes to advance implementation: dose control, evaluation under continuous operation, catalyst management, washing protocols, and coupling the HFT step with conventional downstream biological treatment. Collectively, the results support PBNP/γ-Al_2O_3 as an appropriate catalyst for textile wastewater pretreatment for integration into hybrid AOP–biological schemes and outline concrete actions to validate performance at a larger scale and under variable real effluents.

Author Contributions: Conceptualization, L.I.D. and M.A.A.; methodology, L.I.D., A.M.F.O. and M.A.A.; validation, L.I.D., A.M.F.O. and M.A.A.; investigation, L.I.D. and A.M.F.O.; writing—original draft preparation, L.I.D. and M.A.A.; writing—review and editing, L.I.D., M.C.C. and M.A.A.; visualization, L.I.D.; funding acquisition, L.I.D. and M.A.A. All authors have read and agreed to the published version of the manuscript.

Funding: The authors acknowledge financial support from the UNMdP (800 202405 00025 MP), CONICET (PIP 1220200102822CO, PIBAA 28720210100663CO), and ANPCyT (PICT-2021-CAT-I-00086) which supported the experimental work, reagents, and characterization services associated with this study.

Data Availability Statement: The raw data supporting the conclusions of this article will be made available by the authors upon request.

Acknowledgments: The authors gratefully acknowledge the facilities and technical support provided by INTEMA (CONICET-UNMdP) and ITAPROQ (CONICET-UBA). We are especially grateful to Dr. Mariela De Simone for her valuable and insightful assistance in performing and interpreting the Raman analyses. During the preparation of this manuscript, the authors used ChatGPT (GPT-5; OpenAI) to make superficial improvements to wording and style. The authors have reviewed and edited the output and take full responsibility for the content of this publication.

Conflicts of Interest: The authors declare no conflicts of interest. The funders had no role in the design of the study; in the collection, analyses, or interpretation of data; in the writing of the manuscript; or in the decision to publish the results.

References

1. Holkar, C.R.; Jadhav, A.J.; Pinjari, D.V.; Mahamuni, N.M.; Pandit, A.B. A Critical Review on Textile Wastewater Treatments: Possible Approaches. *J. Environ. Manag.* **2016**, *182*, 351–366. [CrossRef]
2. Jamil, T. Role of Advance Oxidation Processes (AOPs) in Textile Wastewater Treatment: A Critical Review. *Desalination Water Treat.* **2024**, *318*, 100387. [CrossRef]

3. Hanela, S.D.; Fantoni, S.; Cainzos, V.; Ávalos, J.I.; Díaz, S.N.; Romero, E.A.; Vezzoni, A.I.; Candal, R.J.; Miró, E. Removal of Reactive Black 5 from Textile Wastewater by Ozone and Photo-Fenton—Influence of Industrial Matrix Effects. *Lat. Am. Appl. Res.* **2020**, *50*, 101–107. [CrossRef]
4. Christian, D.; Gaekwad, A.; Dani, H.; Shabiimam, M.A.; Kandya, A. Recent Techniques of Textile Industrial Wastewater Treatment: A Review. *Mater. Today Proc.* **2023**, *77*, 277–285. [CrossRef]
5. Herrera-Ibarra, L.-M.; Martín-Domínguez, A.; Ramírez-Zamora, R.-M.; Pérez-Castrejón, S.; Rivera-Huerta, M.-L.; Drogui, P.; Bañuelos-Díaz, J.-A. Electrochemical Peroxidation for the Bleaching of Real Textile Effluents. *J. Environ. Chem. Eng.* **2023**, *11*, 110509. [CrossRef]
6. Doumic, L.I.; Soares, P.A.; Ayude, M.A.; Cassanello, M.; Boaventura, R.A.R.; Vilar, V.J.P. Enhancement of a Solar Photo-Fenton Reaction by Using Ferrioxalate Complexes for the Treatment of a Synthetic Cotton-Textile Dyeing Wastewater. *Chem. Eng. J.* **2015**, *277*, 86–96. [CrossRef]
7. Sun, B.; Zheng, Y.; Shang, C.; Yin, R. Concentration-Dependent Chloride Effect on Radical Distribution and Micropollutant Degradation in the Sulfate Radical-Based AOPs. *J. Hazard. Mater.* **2022**, *430*, 128450. [CrossRef] [PubMed]
8. Wang, J.; Wang, S. Effect of Inorganic Anions on the Performance of Advanced Oxidation Processes for Degradation of Organic Contaminants. *Chem. Eng. J.* **2021**, *411*, 128392. [CrossRef]
9. Ramos, M.D.N.; Santana, C.S.; Velloso, C.C.V.; Da Silva, A.H.M.; Magalhães, F.; Aguiar, A. A Review on the Treatment of Textile Industry Effluents through Fenton Processes. *Process Saf. Environ. Prot.* **2021**, *155*, 366–386. [CrossRef]
10. Kuchtová, G.; Herink, P.; Herink, T.; Chýlková, J.; Mikulášek, P.; Dušek, L. From Lab-Scale to Pilot-Scale Treatment of Real Wastewater from the Production of Rayon Fiber. *Process Saf. Environ. Prot.* **2023**, *171*, 834–846. [CrossRef]
11. Ribeiro, J.P.; Nunes, M.I. Recent Trends and Developments in Fenton Processes for Industrial Wastewater Treatment—A Critical Review. *Environ. Res.* **2021**, *197*, 110957. [CrossRef] [PubMed]
12. Ozturk, D.; Gülcan, M. Synthesis, Characterization, and in-Situ H_2O_2 Generation Activity of Activated Carbon/Goethite/Fe_3O_4/ZnO for Heterogeneous Electro-Fenton Degradation of Organics from Woolen Textile Wastewater. *J. Ind. Eng. Chem.* **2023**, *122*, 251–263. [CrossRef]
13. Esteves, B.M.; Rodrigues, C.S.D.; Madeira, L.M. Wastewater Treatment by Heterogeneous Fenton-Like Processes in Continuous Reactors. In *Applications of Advanced Oxidation Processes (AOPs) in Drinking Water Treatment*; Gil, A., Galeano, L.A., Vicente, M.Á., Eds.; The Handbook of Environmental Chemistry; Springer International Publishing: Cham, Switzerland, 2017; Volume 67, pp. 211–255, ISBN 978-3-319-76881-6.
14. Li, C.; Xu, X.; Liu, M.; He, S.; Qian, Y.; Li, Z. Treatment of High-Salinity Organic Wastewater by Advanced Oxidation Processes: Research Progress and Prospect. *J. Water Process Eng.* **2024**, *60*, 105272. [CrossRef]
15. Liu, X.; Cao, Y.; Sun, J. Defect Engineering in Prussian Blue Analogs for High-Performance Sodium-Ion Batteries. *Adv. Energy Mater.* **2022**, *12*, 2202532. [CrossRef]
16. Liu, J.; Shen, Z.; Lu, C.-Z. Research Progress of Prussian Blue and Its Analogues for Cathodes of Aqueous Zinc Ion Batteries. *J. Mater. Chem. A* **2024**, *12*, 2647–2672. [CrossRef]
17. Sterzinger, J.; Streng, R.; Chen, S.; Götz, R.; Hu, W.; Li, J.; Bandarenka, A.S. Degradation Mechanisms of Prussian Blue Analogues and State-of-the-Art Approaches for Stability Optimization: A Review. *J. Phys. Chem. C* **2025**, *129*, 7135–7153. [CrossRef]
18. Doumic, L.I.; Salierno, G.; Ramos, C.; Haure, P.M.; Cassanello, M.C.; Ayude, M.A. "Soluble" vs. "Insoluble" Prussian Blue Based Catalysts: Influence on Fenton-Type Treatment. *RSC Adv.* **2016**, *6*, 46625–46633. [CrossRef]
19. Salierno, G.; Napoleone, S.; Maisterrena, M.A.; Cassanello, M.; Pellasio, M.; Doumic, L.; Ayude, M.A. Continuous Heterogeneous Fenton-Type Process for Dye Pollution Abatement Intensified by Hydrodynamic Cavitation. *Ind. Eng. Chem. Res.* **2021**, *60*, 16653–16664. [CrossRef]
20. Raman, C.D.; Kanmani, S. Textile Dye Degradation Using Nano Zero Valent Iron: A Review. *J. Environ. Manag.* **2016**, *177*, 341–355. [CrossRef]
21. Doumic, L.; Salierno, G.; Cassanello, M.; Haure, P.; Ayude, M. Efficient Removal of Orange G Using Prussian Blue Nanoparticles Supported over Alumina. *Catal. Today* **2015**, *240*, 67–72. [CrossRef]
22. Sandell, E.B. *Colorimetric Determination of Traces of Metals*, 3rd ed.; Interscience Publishers Inc.: New York, NY, USA, 1959.
23. Chakrabarti, M.H.; Roberts, E.P.L. Analysis of Mixtures of Ferrocyanide and Ferricyanide Using UV-Visible Spectroscopy. *J. Chem. Soc. Pak.* **2008**, *30*, 817.
24. *ISO 8192*; Water Quality-Test for Inhibition of Oxygen Consumption by Activated Sludge. ISO: Geneva, Switzerland, 1995.
25. Samain, L.; Gilbert, B.; Grandjean, F.; Long, G.J.; Strivay, D. Redox Reactions in Prussian Blue Containing Paint Layers as a Result of Light Exposure. *J. Anal. At. Spectrom.* **2013**, *28*, 524. [CrossRef]
26. Moretti, G.; Gervais, C. Raman Spectroscopy of the Photosensitive Pigment Prussian Blue. *J. Raman Spectrosc.* **2018**, *49*, 1198–1204. [CrossRef]
27. Concina, I. An Old Material for a New World: Prussian Blue and Its Analogues as Catalysts for Modern Needs. *Inorganics* **2024**, *12*, 124. [CrossRef]

28. Chen, Y.; Miller, C.J.; Waite, T.D. Heterogeneous Fenton Chemistry Revisited: Mechanistic Insights from Ferrihydrite-Mediated Oxidation of Formate and Oxalate. *Environ. Sci. Technol.* **2021**, *55*, 14414–14425. [CrossRef]
29. Doumic, L.I.; Haure, P.M.; Cassanello, M.C.; Ayude, M.A. Mineralization and Efficiency in the Homogeneous Fenton Orange G Oxidation. *Appl. Catal. B Environ.* **2013**, *142–143*, 214–221. [CrossRef]
30. Chua, Y.T.; Stair, P.C.; Wachs, I.E. A Comparison of Ultraviolet and Visible Raman Spectra of Supported Metal Oxide Catalysts. *J. Phys. Chem. B* **2001**, *105*, 8600–8606. [CrossRef]
31. Hanesch, M. Raman Spectroscopy of Iron Oxides and (Oxy)Hydroxides at Low Laser Power and Possible Applications in Environmental Magnetic Studies. *Geophys. J. Int.* **2009**, *177*, 941–948. [CrossRef]

Disclaimer/Publisher's Note: The statements, opinions and data contained in all publications are solely those of the individual author(s) and contributor(s) and not of MDPI and/or the editor(s). MDPI and/or the editor(s) disclaim responsibility for any injury to people or property resulting from any ideas, methods, instructions or products referred to in the content.